ELSEVIER

J. Non-Newtonian Fluid Mech. 92 (2000) 151–166

Journal of Non-Newtonian Fluid Mechanics

www.elsevier.com/locate/jnnfm

The steady shear of three-dimensional wet polydisperse foams

B.S. Gardiner, B.Z. Dlugogorski*, G.J. Jameson

Department of Chemical Engineering, The University of Newcastle, Callaghan, NSW 2308, Australia

Received 20 July 1999; received in revised form 4 February 2000

Abstract

In this paper, steady shear results are presented from simulations of three-dimensional, polydisperse, wet foams. The simulations use the bubble dynamics model to obtain steady shear results over a wide range of gas fractions, shear rates, and for two normal bubble size distributions. Bingham plastic behaviour is observed in all foams with gas volume fraction above the critical packing fraction of randomly packed hard spheres. Time averaged stress results are seen to be independent of the bubble size distribution. The predicted yield stress behaviour compares favourably with experimental yield stress measurements by previous authors. Shear may increase or decrease the level of topological disorder of foam depending on the foam polydispersity. The present data indicate that shear-induced topological ordering occurs because of insufficient time available for bubbles to pack efficiently in a sheared foam.
© 2000 Elsevier Science B.V. All rights reserved.

Keywords: Steady shear; Polydispersity; Wet foams; Bubble dynamics

1. Introduction

A practical goal for those modelling the rheology of foams and concentrated emulsions is to develop a model that can describe observed behaviour of these two-phase materials. From this perspective, one requires a three-dimensional (3D) model capable of accounting for effects of foam structural properties such as the bubble size distribution, disorder, and a finite liquid fraction, on foam rheology.

Early attempts at modelling the behaviour of foams and concentrated emulsions focused on two-dimensional (2D) systems comprising of monodispersed bubble sizes, with a gas fraction at the dry foam limit (ϕ=1) [1,2]. Dry 2D models were later developed to account for polydisperse bubbles [3–8].

In comparison to the relatively large amount of work on modelling 2D dry foams, little research has been devoted to 3D foams. This is partly due to the relative structural simplicity of 2D foams. In 2D, films joining vertices are represented by curved lines with a single radius of curvature. However in 3D, curved surfaces replace the lines found in 2D. Three curved surfaces meet at a Plateau border and four

* Corresponding author. Tel.: +61-2-4921-6176; fax: +61-2-4921-6920.
E-mail address: cgbzd@alinga.newcastle.edu.au (B.Z. Dlugogorski)

0377-0257/00/$ – see front matter © 2000 Elsevier Science B.V. All rights reserved.
PII: S0377-0257(00)00102-6

Plateau borders meet at a vertex, hence, in general, there are more than one radii of curvature to consider. Difficulties in visualising and observing 3D bubble structural rearrangements in both simulations and experiments have also hampered progress in studying 3D foams.

Reinelt and Kraynik [9] examined the elastic behaviour of a dry, monodisperse 3D foam by considering Kelvin's minimum tetrakaidecahedron. Reinelt [10], using an approximation to the Kelvin cell of planar surfaces with corner angles approximating the correct vertex angles, looked at strains beyond the elastic limit. Later, by applying the Brakke surface evolver program [11] to find minimum surfaces with correct vertex angles, Reinelt and Kraynik [12,13] repeated their previous large strain calculations [10], removing the approximations involved. The general application of the surface evolver program to wet foams and the rheology of wet foams is, for now, limited by the computational requirements. However, progress in this direction is starting to be made [14,15].

A finite liquid content was introduced into 2D models of monodisperse foam by Princen [16,17], Reinelt and Kraynik [18], and Li et al. [19]. Li et al. [19] and Buzza et al. [20] considered explicitly the motion of liquid in vertices and Plateau borders in a sheared foam. A finite liquid fraction was included in 2D polydisperse (disordered) foam models by Bolton and Weaire [21–23] and Hutzler and Weaire [24], through the decoration of vertices with liquid. Durian [25,26] has taken a different approach to modelling foam than previous authors. He proposed formulating a model at the limit of close packing of hard spheres ϕ_c, that is a model of spherical-bubble wet foam, and then extending it to describe the behaviour of polyhedral-bubble foams.

Durian's model allows for a finite liquid fraction, and a distribution of bubble sizes. The foam is modelled as a system of overlapping discs with forces between bubbles proportional to this overlap. The motion of each bubble is predicted by considering the viscous dissipation and compression forces on each bubble. The interaction and motion of an ensemble of bubbles forms the bubble dynamics model.

In this paper, we use a 3D extension to Durian's original bubble dynamics model to study the rheology of wet polydisperse foams. This extension requires special handling of the repulsive forces between bubbles in 3D, and necessitates the calculation of a stress tensor from velocities and positions of single bubbles. The next section introduces the computational methodology, and is followed by a description and discussion of steady shear results. The paper concludes with a summary of its main findings.

2. The bubble dynamics simulation method

In detail, the bubble dynamics model assumes that inertial effects on bubble motion are insignificant in comparison to the effects of inter-bubble compression forces and dissipation in the thin films separating moving bubbles. Therefore at every time-step, the sum of forces on the *i*th bubble is zero,

$$\vec{F}_i^{\text{drag}} + \vec{F}_i^{\text{neigh}} = \vec{0}. \tag{1}$$

Following Durian [25,26], the force on bubble *i* due to the shearing in thin films, by relative motion between neighbouring bubbles, is approximated by

$$\vec{F}_i^{\text{drag}} = -\frac{C\eta_w \langle R\rangle^2}{\delta} \sum_j \left(\vec{v}_i - \vec{v}_j\right) = -bn_i \left(\vec{v}_i - \langle \vec{v}_j \rangle\right), \tag{2}$$

where the total area of a bubble covered by thin films is $A_t = C\langle R\rangle^2$, and $b = A_t\eta_w/\delta$. In Eq. (2), $\langle\vec{v}_j\rangle$ is used to represent the average velocity of neighbouring bubbles.

In Eq. (1), $\vec{F}_i^{\text{neigh}}$ represents the total force on bubble i due to compression from contacting neighbouring bubbles and is determined by summing the pairwise forces $\vec{F}_{ij}$ between all bubble pairs in the simulation system within each time step. The form of the force between contacting bubbles will be discussed in more detail later. For now, it is readily seen that the substitution of Eq. (2) in Eq. (1) yields an equation of motion for each bubble,

$$\vec{v}_i = \langle\vec{v}_j\rangle + \frac{1}{bn_i}\sum_{\substack{j=1\\ j\neq i}}^{N}\vec{F}_{ij}, \tag{3}$$

where the sum of forces on the ith bubble is taken over contacting bubbles (neighbours) only. For a system of bubbles undergoing steady shear, we approximate $\langle\vec{v}_j\rangle$ in Eq. (3) by a linear strain gradient. That is, $\langle\vec{v}_j\rangle = y_i\dot{\gamma}\hat{x}$, where y_i is the position of bubble i in the Y-direction with the bubble system being sheared in the X–Y plane. Note that when $n_i = 0$, $\vec{F}_{ij} = 0$ and $\vec{v}_i = \langle\vec{v}_j\rangle$. The liquid in the thin films is assumed to display Newtonian behaviour.

The force $\vec{F}_{ij}$ between a bubble pair in Durian's 2D simulations is approximated using a spring potential, with the force between contacting bubbles being proportional to the degree of overlap of the circular discs. This spring force is a function of bubble position and radius only. In 3D systems, the spring-like interaction needs to be modified, as it has been found that for 3D spherical bubbles under compression the excess surface energy is also a function of the number of compression sites on a bubble surface.

Whilst modelling the deformation of spherical incompressible droplets by a number of flat surfaces, Lacasse et al. [27,28] discovered that the excess surface energy per compressing surface is a function of the number of these surfaces. Furthermore, Lacasse et al. [27] provided an empirical relation to enable the excess surface energy per bubble contact to be calculated. This empirical excess surface energy expression has the following form

$$\frac{E_i}{n_i} = \frac{4\pi R_i^2 F_o\, c_i(n_i)}{\langle R\rangle}\left[\left(\frac{1}{1-\xi_i}\right)^3 - 1\right]^{\alpha_i(n_i)}, \tag{4}$$

where ξ_i is the nondimensional bubble compression, and $F_o = \sigma\langle R\rangle$. The constants $c_i(n_i)$ and $\alpha_i(n_i)$ are functions of n_i, the number of compressing surfaces or contacting neighbours on bubble i, and are listed in Table 1. By differentiating Eq. (4) with respect to the dimensional compression $R_i\xi_i$, an expression for the restoring (repulsive) force due to a single compression surface is found to be

$$\vec{F}_{\xi i} = \frac{12\pi R_i F_o c_i(n_i)\alpha_i(n_i)}{\langle R\rangle}\left[\left(\frac{1}{1-\xi_i}\right)^3 - 1\right]^{\alpha_i(n_i)-1}\frac{1}{(1-\xi_i)^4}\frac{\vec{r}_i - \vec{r}_j}{|\vec{r}_i - \vec{r}_j|}. \tag{5}$$

The total compression between an overlapping bubble pair is simply the sum of compressions of each bubble, that is

$$(R_i + R_j)\xi_{ij} = R_i\xi_i + R_j\xi_j, \tag{6}$$

Table 1
Empirical contacting neighbour number dependent constants obtained by Lacasse et al. [27] and used to evaluate the bubble interaction force in Eq. (5)

Configuration of contacting surfaces	n_i	$c_i(n_i)$	$\alpha_i(n_i)$
Parallel plates	2	0.007	2.1
Two pair of perpendicular plates	4	0.012	2.1
Tetrahedron	4	0.014	2.1
Cube	6	0.021	2.2
Octahedron	8	0.027	2.3
Rhombic dodecahedron	12	0.055	2.5
Pentagonal dodecahedron	12	0.054	2.5
Icosahedron	20	0.069	2.6

where

$$\xi_{ij} = \frac{R_i + R_j - \left|\vec{r}_i - \vec{r}_j\right|}{R_i + R_j}. \tag{7}$$

If the interacting bubble pair is treated as springs in series, the interaction force may be determined from

$$\vec{F}_{ij} = \vec{F}_{\xi i} = -\vec{F}_{\xi j}. \tag{8}$$

Eqs. (5)–(8) can be solved for ξ_i, ξ_j and $\vec{F}_{ij}$.

The calculation of ξ_i and ξ_j from Eqs. (5)–(8) is not straightforward, as it needs to be done numerically for each neighbour pair at each time step. We found that these rigorous calculations are very time consuming. Therefore, in keeping with the spirit of the simple bubble dynamics simulations in 2D, in this paper we use a more efficient and simpler process for evaluating $\vec{F}_{ij}$, than the solution of Eqs. (5)–(8). The force between bubbles i and j is simply approximated as

$$\vec{F}_{ij} = \frac{6\pi(R_i + R_j)F_o\, c_{av}\, \alpha_{av}}{\langle R\rangle}\left[\left(\frac{1}{1-\xi_{ij}}\right)^3 - 1\right]^{\alpha_{av}-1} \frac{1}{\left(1-\xi_{ij}\right)^4}\frac{\vec{r}_i - \vec{r}_j}{\left|\vec{r}_i - \vec{r}_j\right|}, \tag{9}$$

where α_{av} and c_{av} are the average value of these parameters between the i and j bubble pair, that is $\alpha_{av}=0.5[\alpha_i(n_i)+\alpha_j(n_j)]$ and $c_{av}=0.5[c_i(n_i)+c_j(n_j)]$.

Eq. (9) gives qualitatively the same relationship between bubble overlap and $\vec{F}_{ij}$ as the solution to Eqs. (5)–(8). More importantly, Eq. (9) and the more computationally intensive method of numerically solving Eqs. (5)–(8) are found to give the same time averaged properties of the sheared foam. However, using Eq. (9) requires 5–10 times less CPU time.

From Eqs. (3) and (5), a characteristic time scale for bubble motion may be defined by $\tau_d = b\langle R\rangle/F_o$ In all simulations we set $\tau_d=1$, as done by others [25,26,29]. When the shear rate is scaled by τ_d, then viscous dissipation controls bubble motion for $\dot{\gamma}\tau_d>1$, whereas for $\dot{\gamma}\tau_d<1$ the motion is governed by compression forces, via neighbour interactions.

We would like to make a remark about the capillary number, which reflects the ratio of viscous and surface tension forces. In the context of the present simulations, this number arises as a natural consequence of the interaction between the spring potential and the bubble motion. It is not a priori defined parameter

as used, for example, in boundary integral models of emulsions. The capillary number is related to τ_d and can be obtained by multiplying τ_d by $n_i\left(\vec{v}_i - \langle\vec{v}_j\rangle\right)/\langle R\rangle$.

The advantages of using the bubble dynamics model to simulate foam is not limited to the ease of introducing a bubble size distribution, liquid content, dissipation mechanisms, and extension to 3D. The actual simulation methodology holds additional advantages. As motion of the bubble ensemble is simulated in the same fashion as non-equilibrium molecular dynamics (NEMD) simulation, many of the pre-existing computationally efficient algorithms of NEMD may be employed. These include periodic boundary conditions, to reduce the effect of a relatively small simulation system sizes, linked lists to avoid sorting through non-contacting neighbours at each time step, and the Lees and Edwards shear boundary conditions [30].

As we are endeavouring to simulate 3D systems over a wide range of shear rates, efficient simulation algorithms are crucial, since the number of equations and neighbours per bubble have increased remarkably in comparison to the 2D case. Therefore, to minimise the computational effort, we use periodic boundary conditions in all three directions, as done for example by Dlugogorski et al. [31], in contrast to some simulations, in which a layer of bubbles is fixed at the wall in one direction whilst periodic boundary conditions are used in the other directions [25,26,29,32].

A Verlet neighbour list [30] is used to quickly find contacting bubble neighbours for each bubble. At each time step during the simulation we evaluate forces between contacting neighbour pairs. To avoid searching through the entire system of bubbles for contacting neighbours, neighbour lists are created for each bubble. The neighbour list consists of bubbles within a cut-off radius of the *i*th bubble. Neighbour lists significantly reduce search times and therefore computation time.

Initially bubbles are assigned to positions on a face-centred-cubic crystalline lattice. Bubbles are then allocated radii randomly according to the specified bubble size distribution function. Subsequently, the volume of the sparse cubic lattice is decreased until the desired gas volume fraction is achieved. Before the bubble system is sheared, it is first equilibrated by setting $\langle\vec{v}_j\rangle = \vec{0}$ and then applying Eq. (3) to determine bubble velocities. New bubble positions are determined from the calculated velocities. This procedure is repeated until the sum of compressive forces on each bubble from neighbouring bubbles is zero ($\vec{F}_i^{\text{neigh}} = \vec{0}$) to within numerical accuracy. Bubble positions are updated using $\vec{r}_i(t + \Delta t) = \vec{r}_i(t) + 0.5[\vec{v}_i(t) + \vec{v}_i(t + \Delta t)]\Delta t$ during equilibration and shear.

In the present study the number of neighbours for each bubble are calculated at each time step, and the constants $c_i(n_i)$ and $\alpha_i(n_i)$ are determined from a numerical fit to the data in Table 1, that is,

$$c_i(n_i) = 1.68 \times 10^{-3} + 6.74 \times 10^{-4} n_i + 5.52 \times 10^{-4} n_i^2 - 2.08 \times 10^{-5} n_i^3; \tag{10}$$

$$\alpha_i(n_i) = 1.96 + 5.20 \times 10^{-2} n_i - 9.28 \times 10^{-4} {n_i}^2. \tag{11}$$

The two bubble size distributions used in the following set of simulations are illustrated in Fig. 1. For all results presented, the number of bubbles used is 256. We also performed simulations with 500 and 1372 bubbles to confirm that time averaged results are independent of system size. Although fluctuations increase with a decreasing system size, it was necessary to use the smaller system size of 256 bubbles to conduct large-strain computations at very low shear rates. The simulations take between 60 min and 7 days, for the very high and very low shear rates, respectively, on a 300 MHz Pentium-based computer.

In the following simulations, shear is imposed using the Lees and Edwards boundary condition, which alters the periodic boundary condition in the *Y* direction to mimic shear [30]. For shearing in the *X*–*Y* plane, if a bubble leaves the simulation box in the *Y*-direction it re-enters through the opposite side of the

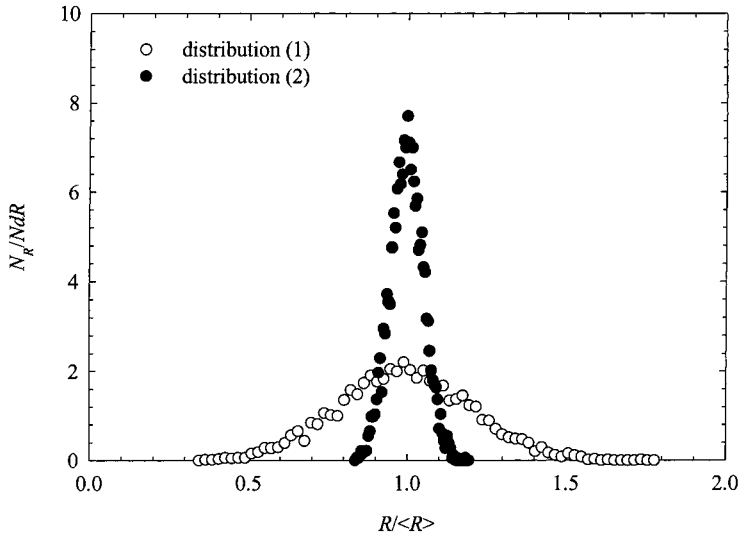

Fig. 1. Illustration of two normal bubble size distributions considered throughout simulations.

simulation box. However, its position is displaced in the X-direction and its X-velocity changed according to the imposed shear rate. The standard periodic boundary conditions are applied in X and Z directions. This means that a bubble leaving the simulation box either in the X or Z direction re-enters through the opposite side of the box with its X or Z co-ordinate adjusted accordingly, but without alteration to its velocity. Fig. 2 illustrates the response of a 2D bubble system to the imposed Lees and Edwards shear. The degree of bubble overlap, and hence the overall stress of the system, increases significantly as bubbles are

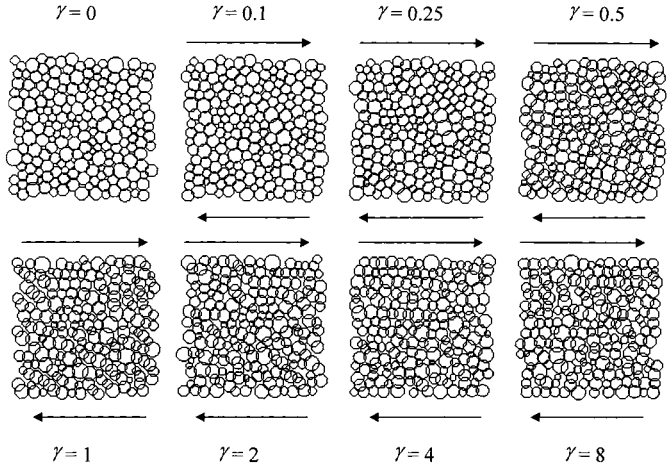

Fig. 2. Images of a 2D bubble dynamics simulations of a shearing foam; N=200, ϕ=0.95, $\dot{\gamma}\tau_d$=1, distribution (1). For clarity this figure presents the results from 2D computations rather than from 3D runs, as discussed elsewhere in the paper. This is done to illustrate the overlapping bubbles, which reflect bubble elongation, as a consequence of imposed shearing and the Lees and Edwards periodic boundary condition.

forced to move relative to one another. Note that the increased overlapping of the bubbles in the system implies bubble elongation in the direction of no overlap.

The stress tensor is determined using the following expression

$$\tau = \frac{1}{V}\sum_{ij}(\vec{r}_i - \vec{r}_j)\vec{F}^{\mathrm{s}}_{ij}, \tag{12a}$$

where V is the volume of the computational box, $\vec{F}^{\mathrm{s}}_{ij}$ is the sum of compressional bubble forces and the pair hydrodynamic forces between each bubble-neighbour pair [33]. Eq. (12a) can be rewritten as

$$\tau = \frac{1}{V}\left[\sum_{ij}(\vec{r}_i - \vec{r}_j)\vec{F}_{ij} + b\sum_{ij}(\vec{r}_i - \vec{r}_j)(\vec{v}_j - \vec{v}_i)\right]. \tag{12b}$$

The foam viscosity is determined from the time averaged X–Y component of the stress tensor

$$\eta = -\frac{\langle\tau_{xy}\rangle}{\dot{\gamma}}. \tag{13a}$$

We also compute the other viscometric functions, namely the first and second normal stress differences,

$$N_1 = \tau_{xx} - \tau_{yy}, \tag{13b}$$

$$N_2 = \tau_{yy} - \tau_{zz}. \tag{13c}$$

3. Bubble dynamics model's prediction of steady shear rheology of foams

Figs. 3–5 illustrate the response of the model foam to the onset of strain for two bubble size distributions. In Fig. 3, for both bubble size distributions, τ_{xy} initially increases with strain, almost linearly, until a yield strain is exceeded (with a corresponding yield stress), and then the stress fluctuates about an average value. The time average of the fluctuations provides the value of the shear stress of the foam undergoing steady shear. For the wide bubble size distribution (distribution (1)) the yield stress only slightly exceeds the steady-state stress, whereas for the narrow distribution (distribution (2)) there is a significant difference between the yield stress and the steady-state stress.

Figs. 4 and 5 show the initial behaviour of the normal stress differences and excess surface energy. In contrast to the linear small strain behaviour of τ_{xy} in Fig. 3, the N_1, N_2 and excess surface energy all increase in a parabolic trend up to the yield strain. This behaviour has been observed previously in 2 and 3D dry foam models [5,7,10].

We observe that the time averaged stress, at a given shear rate and gas fraction, is independent of the bubble size distribution of the foam used in the simulation. On the other hand, the small strain behaviour of the narrow bubble size distribution (Figs. 3b and 4b) is what would be expected of a shearing crystal, or any periodic lattice, undergoing a stick-slip motion with bubble rearrangements occurring simultaneously throughout the system. The narrow bubble size distribution allows the bubbles to form a crystalline packing configuration. Bubble rearrangements can occur at well defined strains. This phenomenon has been observed previously in periodic 2 and 3D monodisperse foam models [2,10,13,17,18]. The bubble-dynamics simulation presented here differs from these previous models by allowing structural

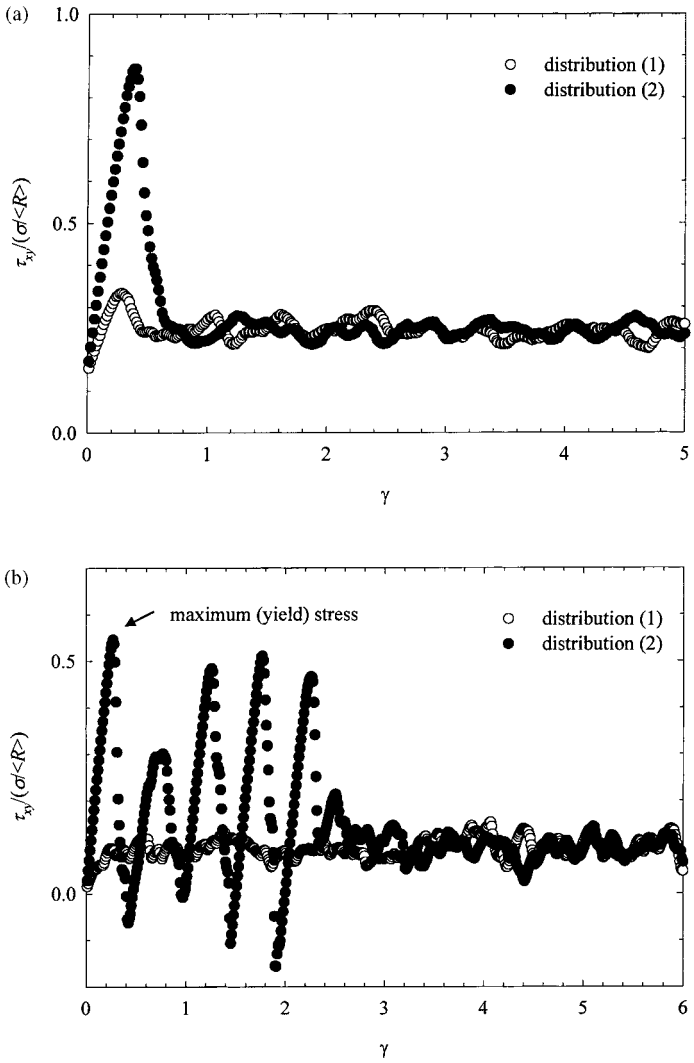

Fig. 3. The initial response of τ_{xy} to the imposed shear for the two bubble size distributions shown in Fig. 1, (a) N=256, ϕ=0.95, $\dot{\gamma}\tau_d$=0.1 and (b) N=256, ϕ=0.95, $\dot{\gamma}\tau_d$=0.01.

disorder to occur. In the present simulations, bubbles can escape from a crystalline arrangement to form a less efficient packing during shear. Disorder causes the well-defined strain rearrangement events to be smeared over a range of strains, until fluctuations appear random.

The results presented in Figs. 3 and 4 (in particular those included in Figs. 3b and 4b) were obtained for foams which were relaxed (equilibrated) from their initial positions on FCC lattice, with a subsequent imposition of shear. However, when shearing simulations were performed for previously sheared (then relaxed) narrow distribution foams, the small-strain stick-slip behaviour was not observed. This indicates that narrow distribution foams form crystalline packing configurations, which tend to be preserved during equilibration runs and are destroyed only during pre-shearing.

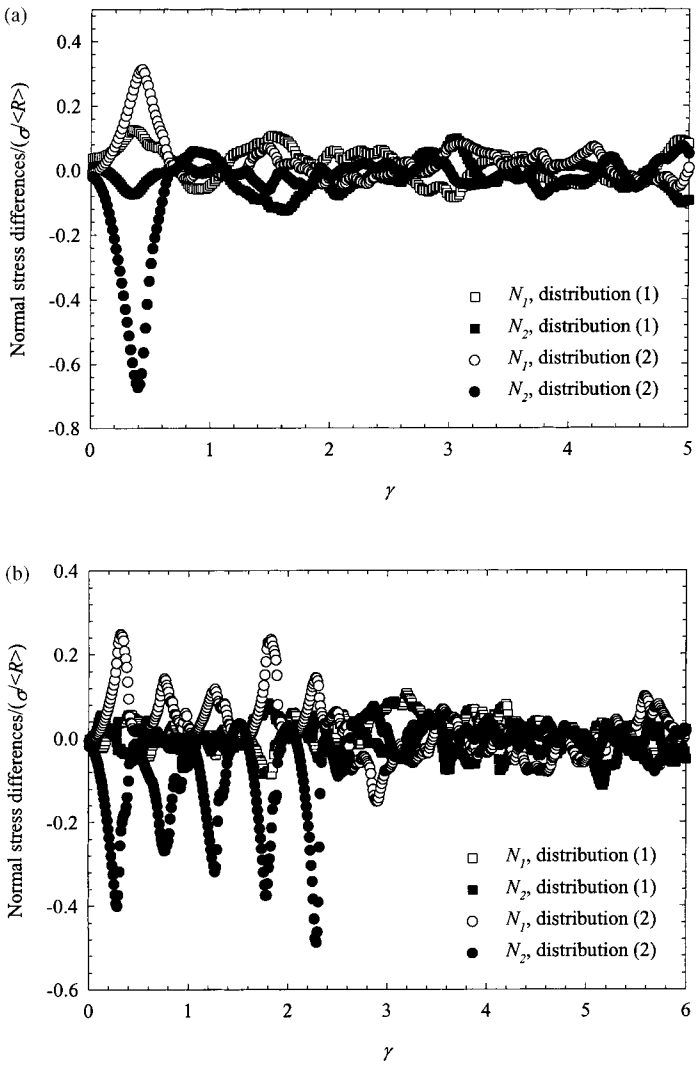

Fig. 4. The initial behaviour of the normal stress differences ($N_1=\tau_{xx}-\tau_{yy}$ and $N_2=\tau_{yy}-\tau_{zz}$) after the onset of shear for the two bubble size distributions shown in Fig. 1; (a) N=256, ϕ=0.95, $\dot{\gamma}\tau_d$=0.1 and (b) N=256, ϕ=0.95, $\dot{\gamma}\tau_d$=0.01.

Bubbles trapped by the close proximity of neighbouring bubbles can be thought of as being trapped by a spatial distribution of energy barriers [34,35]. In the case of the narrow bubble size distribution, shear increases structural disorder and therefore widens the distribution of energy barriers. The independence of steady shear behaviour on polydispersity reflects a similar distribution of energy barriers due to disorder.

Fig. 6 displays the steady shear simulation predictions over a range of gas fractions and shear rates for distribution (1) foam. The time averaged behaviour of distribution (2) foams is identical. The overall steady shear rheology displayed is consistent with a Bingham plastic model, that is

$$\tau_{xy} = \tau_o + k\dot{\gamma}, \tag{14}$$

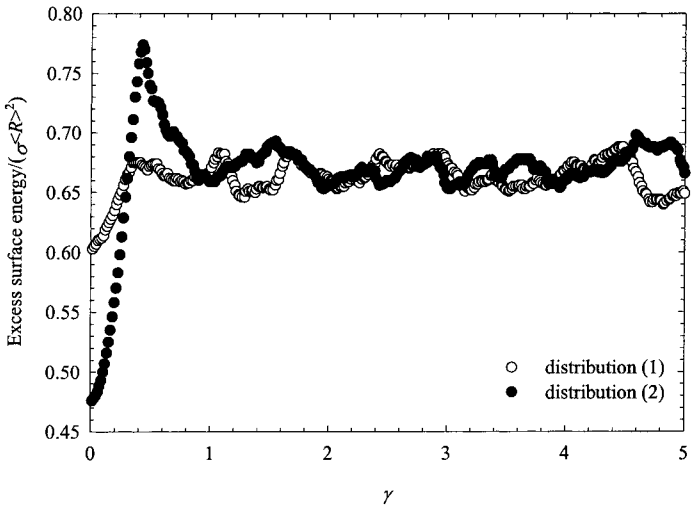

Fig. 5. The initial behaviour of the excess surface energy per bubble after the onset of shear for the two bubble size distributions shown in Fig. 1; N=256, ϕ=0.95, $\dot{\gamma}\tau_d$=0.1.

where τ_o is sometimes called the dynamic yield stress [5] and may be different from the yield stress. At high shear rates, foams at all gas fractions display a shear-rate independent viscosity, as illustrated in Fig. 7. At low shear rates, the shear behaviour of foam is consistent with a plastic fluid. For all shear rates, the viscosity increases with gas fraction. The only foam not showing Bingham plastic behaviour is that with a gas volume fraction of 0.6, which is below the critical packing fraction of hard spheres. In this case, slight shear thinning behaviour is observed at intermediate shear rates, however, there is no indication of

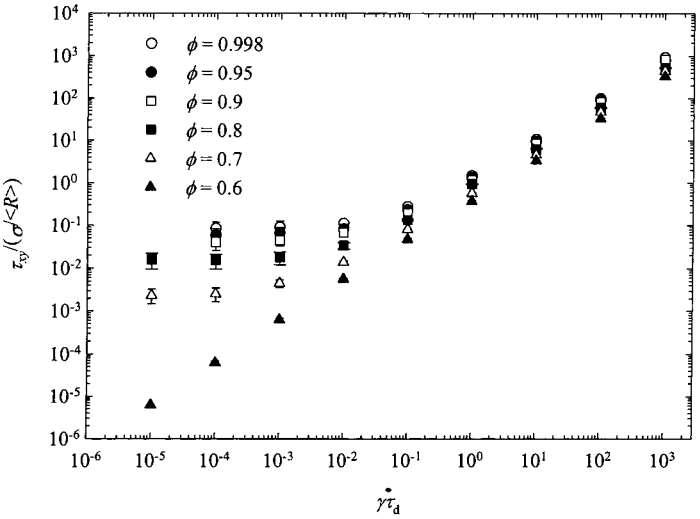

Fig. 6. The time averaged steady shear behaviour of foam of various gas fractions over a range of shear rates. Error bars indicate standard deviation; N=256, distribution (1).

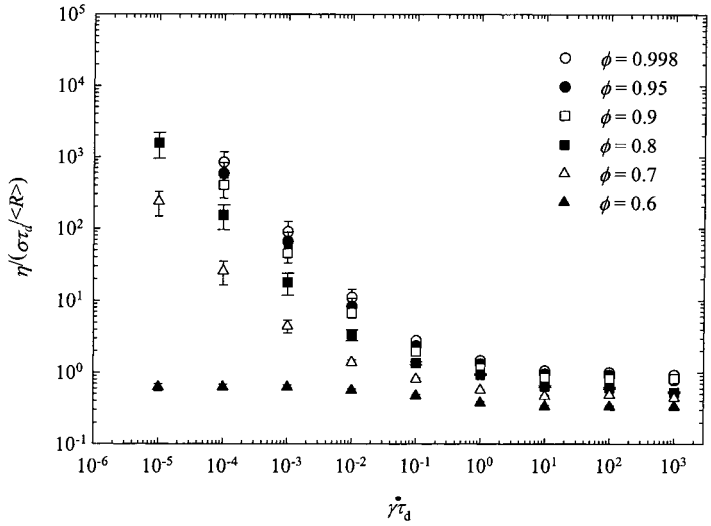

Fig. 7. Viscosity of foam from steady shear simulations at various gas fractions and shear rates. Error bars indicate standard deviation; N=256, distribution (1).

a dynamic yield stress for the shear rates simulated. Note that it is still possible for foams with $\phi<\phi_c$ to display a dynamic yield stress at lower shear rates than available in the present simulations. This is because, near ϕ_c bubbles are still packed tightly enough for neighbouring bubbles to interfere with bubble motion.

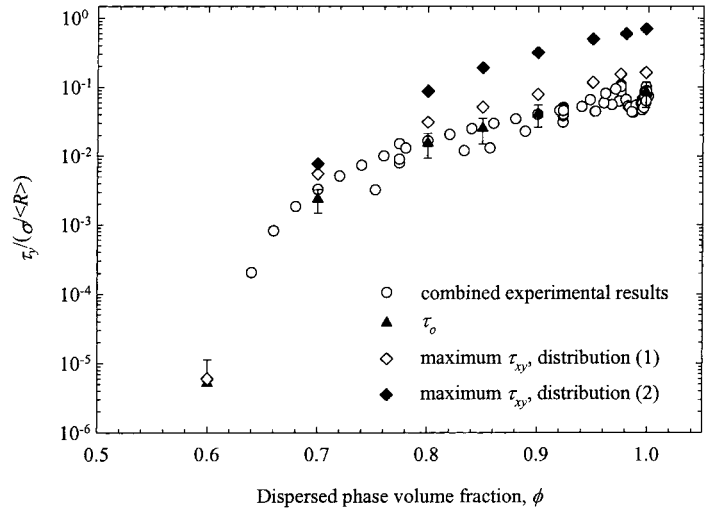

Fig. 8. The dependence of the dynamic yield stress τ_o and maximum stress (at $\dot{\gamma}\tau_d=10^{-4}$) over a range of dispersed phase volume fractions. Experimental concentrated emulsion yield stress results of Princen [36], Yoshimura et al. [37], Princen and Kiss [38] and Mason et al. [39] and the dry foam results of Gardiner et al. [40] are included for comparison. (The latter reference also contains a more detailed comparison of all complete yield-stress data sets, presently known to us, which include information of particle size and surface tension.) Note for $\phi\leq0.7$, the maximum stress is plotted for normalised shear rates of 10^{-5}; N=256. The dynamic yield stress τ_o was obtained by fitting Eq. (15) to the shear predictions illustrated in Fig. 6.

When the dynamic yield stress (time averaged steady shear stress, τ_o) and maximum stress (yield stress) is compared with experimental yield stress results [36–40] (Fig. 8) over a range of gas fractions, the same general trend of increasing yield stress with increasing gas fraction is observed. In particular, the dataset which spans the greatest range of ϕ, the monodisperse concentrated emulsions results of Mason et al. [39], follows

$$\frac{\tau_y}{(\sigma/\langle R\rangle)} = 0.51(\phi - \phi_c)^2, \tag{15}$$

where ϕ_c=0.62 and corresponds approximately to the critical packing fraction of randomly packed hard spheres. We find that the dynamic yield-stress data agree strongly with the results of Mason et al. [39], even at high gas fractions. However, the maximum (yield) stress diverges from experimental results at high gas fractions. At the low gas fractions, in which the bubble dynamics method is most appropriate, good agreement is found between predictions and experimental results.

We now turn our attention to the effect of steady shear on foam microstructure. The average number of contacting neighbours per bubble $\langle n\rangle$ and the second moment of the distribution of contacting neighbours μ_2 may be used to characterise the effect of shear on the microstructure of a foam. Topological disorder is usually defined by μ_2. In some cases it is found that shearing may cause a decrease in topological disorder. As shown in Fig. 9, it is apparent that shearing a narrow bubble size distribution foam increases the topological disorder of the foam system, whereas for the wider distribution foam, shearing actually decreases the level of disorder. For both distributions, an increasing shear rate reduces the average number of neighbours per bubble. Shear induced ordering has been observed previously in simulations of 2D dry foams [5,41].

If a foam is not sheared, the bubbles arrange to give an efficient packing that minimises local bubble compression. With an increase in the shear, bubbles are not allowed sufficient time to pack efficiently.

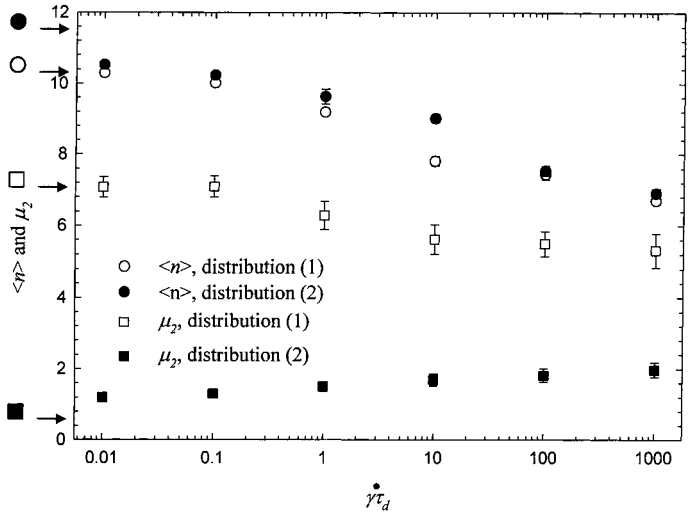

Fig. 9. Variation in the number of contacting bubble neighbours and the second moment of the number of contacting neighbours, as a function of shear rate. Arrow on vertical axis indicate the value of $\langle n\rangle$ and μ_2 of an unsheared foam; N=256, ϕ=0.95.

Instead of a uniform compression from all sides by neighbouring bubbles, a bubble may be held in a position by a larger compressional force from a smaller number of bubbles. In this way, the average number of contacting neighbours is reduced due to shear. An unsheared foam with a narrow bubble size distribution may have a crystal-like microstructure with a low level of μ_2. Shearing will disrupt the crystalline packing and will always increase the level of topological disorder. The decrease in disorder of foam with a wide distribution of bubble sizes is harder to understand.

Weaire et al. [41] proposed that the shear-induced decrease in ordering of foams is due to the dependence of the degree of bubble deformation on the bubble size. Larger bubbles tend to be stretched more than small bubbles in a sheared foam. The number of sides a bubble has depends on the bubble size, on average. Some large many-sided bubbles, in a sheared foam, tend to lose sides with a corresponding increase in the number of fewer sided bubbles. Since large bubbles are more likely to be surrounded by small bubbles (Aboav's law), if a large bubble loses a side a neighbouring small bubble is likely to gain a side. The result is a decrease in the difference between the number of sides of an average large bubble and an average small bubble.

In the bubble dynamics simulation there is no true bubble deformation or thin film elongation. The number of contacting neighbours a bubble has in an unsheared foam depends on bubble size [42]. The number of contacting neighbours per bubble decreases due to inefficient packing of a sheared foam. This decrease in the number of contacting neighbours occurs disproportionately for large many-sided bubbles. In a closely packed system, bubbles will usually have at least two contacts per degree of freedom, that is n=6 in 3D, to support forces in all directions. Large bubbles with additional contacts are capable of losing bubble connections whereas small bubbles will be more likely to retain approximately six contacting neighbour bubbles. This is illustrated in Fig. 10. The result is that the distribution of the number of contacting bubbles is reduced due to a significant reduction in the number of many-sided bubbles.

Dennin and Knobler [43], in experiments on shear flow in a foam monolayer, found that the μ_2 was independent of strain. What is clear from our simulations is that strain can increase or decrease disorder

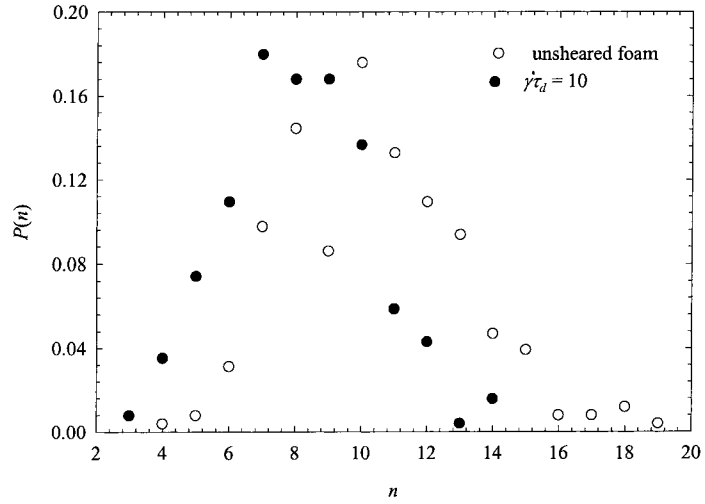

Fig. 10. Comparison of the contacting neighbour distribution of a sheared and unsheared foam; ϕ=0.95, distribution (1), N=256.

depending on either bubble size distribution or degree of disorder. It is possible then to observe no effect of strain on disorder at intermediate bubble size distributions. Furthermore, Dennin and Knobler's experiments were carried out at low non-dimensional shear rates, where we find less of an effect of strain on μ_2 in comparison to the unstrained foam.

Although the degree of topological disorder and average number of neighbours is different for the two distributions studied, the time averaged stress behaviour is identical. As bubble size distribution and μ_2 are clearly related, the independence of the time averaged stress behaviour to μ_2 may be implied. As seen in Figs. 3b and 4b the effect of structural disorder (not topological disorder) is extremely important to foam flow behaviour.

4. Conclusions

In this paper, the bubble dynamics model has been successfully used to predict the steady shear rheology of wet polydisperse 3D foams. The results could also apply to concentrated emulsions. The predicted behaviour is consistent with Bingham plastic behaviour observed in foam experiments [44]. The time average behaviour of foams was found to be independent of the bubble size distribution or topological disorder. However, the behaviour near the onset of strain significantly differs for the two normal distributions studied.

The maximum stress and the dynamic yield stress predicted by the bubble dynamics model were compared with experimental concentrated emulsion and foam yield stress measurements over a range of dispersed phase fractions. Good agreement was found between predictions and experiments at gas fractions near the critical hard sphere packing fraction, a region in which the bubble dynamics model is most suited. At gas fractions approaching the dry foam limit, the maximum stress and experimental yield stress results diverge. However, the dynamic yield stress predictions closely follow the experimental data up to the dry foam limit.

It is observed that shear induced ordering is possible in 3D wet foams. Previously, shear induced topological ordering has been observed in 2D dry foam simulations [5,41]. An explanation for shear-induced ordering is presented based on the bubble size dependence of the number of contacting neighbours per bubble and limitations on the time available to achieve efficient bubble packing.

5. Nomenclature

A_t	surface area covered by thin films for bubble with an average radius (m^2)
b	grouping constant in Eq. (2) ($N\,s\,m^{-1}$)
C	constant in Eq. (2) (–)
$c_i(n_i)$	a constant in 3D bubble interaction force depending on the number of neighbours (–)
c_{av}	average between $c_i(n_i)$ and $c_j(n_j)$ for an interacting bubble pair (–)
E	excess surface energy per bubble (N m)
$\vec{F}_i^{drag}$	sum of drag forces on the ith bubble due to neighbouring bubbles (N)
$\vec{F}_i^{neigh}$	sum of forces on the ith bubble due to compression from neighbouring bubbles (N)
$\vec{F}_{ij}$	the total force between the ith and jth bubble due to compression (N)

$\vec{F}_{ij}^{\mathrm{s}}$	the sum of compressional bubble forces and the pair hydrodynamic forces between a bubble neighbour pair (N)
F_{o}	force constant (N)
$\vec{F}_{\xi i}$	the repulsive force exerted by the *i*th bubble due to compression between the *i*th and *j*th bubble (N)
N	total number of bubbles in the simulation
N_1, N_2	normal stress differences (Pa)
N_R	number of bubbles of radius R (–)
n	number of contacting neighbours (–)
$\langle n \rangle$	average number of contacting neighbours per bubble (–)
$P(n)$	probability of a bubble having n contacting neighbours (–)
R	bubble radius (m)
$\langle R \rangle$	average bubble radius (m)
$\vec{r}$	bubble position (m)
t	time (s)
Δt	simulation time step (s)
V	volume of simulated foam system (m^3)
$\vec{v}$	bubble velocity ($\mathrm{m\,s^{-1}}$)
$\langle \vec{v}_j \rangle$	average velocity of bubbles neighbouring the *i*th bubble ($\mathrm{m\,s^{-1}}$)
$\hat{x}$	unit normal vector in the X-direction (–)
y	Y-position of bubble (m)
$\alpha_i(n_i)$	exponent in 3D bubble interaction force depending on the number of neighbours (–)
α_{av}	average between $\alpha_i(n_i)$ and $\alpha_j(n_j)$ for an interacting bubble pair (–)
δ	thickness of thin film (–)
ϕ	gas volume fraction (–)
ϕ_{c}	maximum packing fraction of randomly packed hard spheres (–)
γ	strain (–)
$\dot{\gamma}$	shear rate (–)
η	foam viscosity (Pa s)
η_{w}	liquid phase viscosity (Pa s)
μ_2	second moment distribution of the number of contacting neighbours per bubble (–)
σ	surface tension ($\mathrm{N\,m^{-1}}$)
τ	stress tensor (Pa)
τ_{d}	bubble rearrangement time-scale (s)
τ_{o}	dynamic yield stress (Pa)
τ_{y}	yield stress (Pa)
$\langle \tau_{xy} \rangle$	time averaged X–Y component of the stress tensor (Pa)
ξ	nondimensional compression (–)

Subscripts

i, j	refer to bubbles i and j, respectively
ij	refers to interaction between bubbles i and j
x, y, z	refer to components of the stress tensor in the X, Y, Z directions, respectively.

Acknowledgements

This investigation was funded by the Australian Research Council.

References

[1] S.A. Khan, R.C. Armstrong, J. Non-Newtonian Fluid Mech. 22 (1986) 1.
[2] A.M. Kraynik, M.G. Hansen, J. Rheol. 31 (1987) 175.
[3] S.A. Khan, R.C. Armstrong, J. Non-Newtonian Fluid Mech. 25 (1987) 61.
[4] A.M. Kraynik, D.A. Reinelt, H.M. Princen, J. Rheol. 35 (1991) 1235.
[5] T. Herdtle, PhD Dissertation, 1991.
[6] T. Herdtle, H. Aref, J. Fluid Mech. 241 (1992) 233.
[7] T. Okuzono, K. Kawasaki, T. Nagai, J. Rheol. 37 (1993) 571.
[8] T. Okuzono, K. Kawasaki, Phys. Rev. E. 51 (1995) 1246.
[9] D.A. Reinelt, A.M. Kraynik, J. Coll. Interf. Sci. 159 (1993) 460.
[10] D.A. Reinelt, J. Rheol. 37 (1993) 1117.
[11] K.A. Brakke, Exp. Math. 1 (1992) 141.
[12] A.M. Kraynik, D.A. Reinelt, J. Colloid Interf. Sci. 181 (1996) 511.
[13] D.A. Reinelt, A.M. Kraynik, J. Fluid Mech. 311 (1996) 327.
[14] D. Weaire, R. Phelan, Phil. Trans. R. Soc. Lond. A 354 (1996) 1989.
[15] A.M. Kraynik, NATO School on Foams, Emulsions, Cellular Materials, Cargése, 1997.
[16] H.M. Princen, J. Colloid Interf. Sci. 71 (1979) 55.
[17] H.M. Princen, J. Colloid Interf. Sci. 91 (1983) 160.
[18] D.A. Reinelt, A.M. Kraynik, J. Fluid Mech. 215 (1990) 431.
[19] X. Li, H. Zhou, C.J. Pozrikidis, J. Fluid Mech. 286 (1995) 379.
[20] D.M.A. Buzza, C.-Y. Lu, M.E. Cates, J. Phys. II France 5 (1995) 37.
[21] F. Bolton, D. Weaire, Phys. Rev. Lett. 65 (1990) 3449.
[22] F. Bolton, D. Weaire, Philos. Mag. B 63 (1991) 795.
[23] F. Bolton, D. Weaire, Philos. Mag. B 65 (1992) 473.
[24] S. Hutzler, D. Weaire, J. Phys. Condens. Matter 7 (1995) L657.
[25] D.J. Durian, Phys. Rev. Lett. 75 (1995) 4780.
[26] D.J. Durian, Phys. Rev. E 55 (1997) 1739.
[27] M.-D. Lacasse, G.S. Grest, D. Levine, T.G. Mason, D.A. Weitz, Phys. Rev. Lett. 76 (1996) 3448.
[28] M.-D. Lacasse, G.S. Grest, D. Levine, Phys. Rev. E 54 (1996) 5436.
[29] S.A. Langer, A.J. Liu, J. Phys. Chem. B 101 (1997) 8667.
[30] M.P. Allen, D.J. Tildesley, Computer Simulations of Liquids, Oxford University Press, New York, 1992.
[31] B.Z. Dlugogorski, M. Grmela, P.J. Carreau, J. Non-Newtonian Fluid Mech. 48 (1993) 303.
[32] B.Z. Dlugogorski, M. Grmela, P.J. Carreau, Rheol. Acta 34 (384) 1995.
[33] R.C. Ball, J.R. Melrose, Physica A 247 (1997) 444.
[34] P. Sollich, F. Lequeux, P. Hébraud, M.E. Cates, Phys. Rev. Lett. 78 (1997) 2020.
[35] P. Sollich, Phys. Rev. E 58 (1998) 738.
[36] H.M. Princen, J. Colloid Interf. Sci. 105 (1985) 150.
[37] A.S. Yoshimura, R.K. Prud'homme, H.M. Princen, A.D. Kiss, J. Rheol. 31 (1987) 699.
[38] H.M. Princen, A.D. Kiss, J. Colloid Interf. Sci. 128 (1989) 176.
[39] T.G. Mason, J. Bibette, D.A. Weitz, J. Colloid Interf. Sci. 179 (1996) 439.
[40] B.S. Gardiner, B.Z. Dlugogorski, G.J. Jameson, R.P. Chhabra, J. Rheol. 42 (1998) 1437.
[41] D. Weaire, F. Bolton, T. Herdtle, H. Aref, Philos. Mag. Lett. 66 (1992) 293.
[42] B.S. Gardiner, B.Z. Dlugogorski, G.J. Jameson, J Phys: Conden. Matter 11 (1999) 5295.
[43] M. Dennin, C.M. Knobler, Phys. Rev. Lett. 78 (1997) 2485.
[44] S.A. Khan, C.A. Schnepper, R.C. Armstrong, J. Rheol. 32 (1988) 69.